Talanta 113 (2013) 62–67

Contents lists available at SciVerse ScienceDirect

Talanta

journal homepage: www.elsevier.com/locate/talanta

Direct deconvolution approach for depth profiling of element concentrations in multi-layered materials by confocal micro-beam X-ray fluorescence spectrometry

Pawel Wrobel*, Mateusz Czyzycki

Faculty of Physics and Applied Computer Science, AGH University of Science and Technology, al. Mickiewicza 30, 30-059 Krakow, Poland

ARTICLE INFO

Article history:
Received 7 February 2013
Received in revised form
27 March 2013
Accepted 29 March 2013
Available online 6 April 2013

Keywords:
Confocal X-ray fluorescence spectroscopy
Chemical imaging
Quantitative analysis
Multi-layered materials
Deconvolution

ABSTRACT

A new approach for the determination of element concentration profiles in stratified materials by confocal X-ray fluorescence spectrometry was elaborated. The method was based on a direct deconvolution of the measured depth-dependent X-ray fluorescence intensity signal with the established response function of the spectrometer. Since the approach neglects the absorption of primary and secondary radiation within the probing volume, it is applicable only to low absorbing samples and small probing volumes. In the proposed approach the deconvolution is performed separately for all detectable elements and it is followed by the correction of absorption effects. The proposed approach was validated by using stratified standard samples. The determined elemental profiles were compared with the results obtained by using existing analytical approaches.

1. Introduction

The confocal micro-beam X-ray fluorescence (confocal μ-XRF) technique is an analytical tool that enables examination of spatial distributions of elements within a sample with a resolution ranging from several up to tens of micrometers. The method was proposed in 1993 by Gibson and Kumakov [1] and since then many authors proved its capability for analyzing samples of different origin, such as pigment layers in art objects or elemental distributions in biological and environmental samples [2–5]. The technique has been used with spectrometers operated either with synchrotron radiation or the radiation generated by X-ray tubes [6–8]. The main advantage of the technique is its capability for collecting depth resolved elemental information with extremely high signal to background ratio arising due to the inherently limited probing volume. The disadvantages include limited sensitivity for high-Z elements and element-dependent spatial resolution, both effects linked to the way in which X-rays are transmitted and reflected in the focusing/collimating optics of the spectrometer. Nevertheless, for certain applications, the technique was found very useful as the only one the technique capable of non-invasive probing the sequence and chemical composition of sample layers. The comparison of the detection limits and elemental sensitivities of conventional μ-XRF versus confocal μ-XRF techniques can be found in [9].

The elaboration of any quantification procedure for confocal μ-XRF technique is a demanding task since the spatial description of the matrix effects inside heterogeneous sample is much more difficult than in the case of conventional XRF. So far a few method were developed. The first quantification procedure for confocal μ-XRF was presented in 2004 by Smit et al. [10]. In this work the fundamental parameter approach assuming a spherical probing volume was proposed for the investigation of paint layers. A more detailed model of confocal volume was proposed by Malzer and Kanngießer in 2005 [11]. The authors also derived a general equation for the depth-dependent intensity of X-ray fluorescence radiation in confocal geometry as well as a calibration procedure. Mantouvalou et al. [12] used this approach to derive the equations describing the intensity of X-ray fluorescence radiation versus the probing depth in multi-layered samples. A Monte Carlo (MC) based quantification approach was presented and compared with the existing analytical methodologies by Czyzycki et al. in two articles [13–14]. Perez et al. [2] applied the model of Malzer and Kanngießer [11], neglecting the self-absorption effects, for the analysis of metals in thin biological samples. Both the analytical and MC approaches used the parallel beam approximation [15]. Schoonjans et al. [16] elaborated a fundamental parameter method for nano-X-ray fluorescence analysis of cometary dust particles trapped in silica-based aerogel returned by NASA's Stardust mission. The analytical approach

* Corresponding author. Tel.: +48 12 6172956; fax: +48 12 6340010.
E-mail address: Pawel.Wrobel@fis.agh.edu.pl (P. Wrobel).

0039-9140/$ - see front matter © 2013 Elsevier B.V. All rights reserved.
http://dx.doi.org/10.1016/j.talanta.2013.03.087

used in our work was based on the initial equation proposed originally by Malzer and Kanngießer in [11].

2. Theory

In the model derived by Malzer and Kanngießer [11] the spectrometer sensitivity function $\eta_j(x)$ was introduced. In this model, depth-dependent intensity of X-ray fluorescence radiation of given element j recorded in confocal geometry, assuming monochromatic excitation, paraxial X-ray optics, and neglecting enhancement effects, is given by:

$$\Phi_j(x) = \int_0^D \eta_j'(\zeta - x)\rho_j(\zeta)\exp\left(-\int_0^\zeta \overline{\mu}_{lin,j}(\xi)d\xi\right)d\zeta, \tag{1}$$

$$\eta_j'(x) = \Phi_0\tau_{F,j}\eta_j(x) = \Phi_0\tau_{F,j}\frac{\tilde{\eta}_j}{\sqrt{2\pi}\sigma_{x,j}}\exp\left(\frac{-x^2}{2\sigma_{x,j}^2}\right), \tag{2}$$

$$\overline{\mu}_{lin,j}(x) = \sum_i \rho_i(x)\left(\frac{\mu_{0,i}}{\cos\varphi} + \frac{\mu_{j,i}}{\cos\psi}\right), \tag{3}$$

where $\tilde{\eta}_j$ takes into account the geometry of the confocal volume and the transmission factors of the excitation/detection X-ray optics and the detection efficiency, $\sigma_{x,j}$ is the width of the sensitivity profile, Φ_0 is the flux of the impinging beam, $\tau_{F,j}$ is the X-ray peak production cross section, φ and ψ are the incidence and take off angles measured to the sample normal, $\mu_{0,i}$ and$\mu_{j,i}$ are the mass absorption coefficients for the primary and secondary radiation. The function $\rho_j(x)$ describes the local density profile of the analyzed element. For thin samples, when the absorption effects can be omitted

$$\Phi_j(x) = \eta_j'(x)Q_j, \tag{4}$$

where Q_j is the mass deposit per unit area of the analyzed element. In the approach proposed in this work the absorption term in Eq. (1) is split in two separate terms:

$$\exp\left(-\int_0^\zeta \overline{\mu}_{lin,j}(\xi)d\xi\right) = \exp\left(\int_\zeta^x \overline{\mu}_{lin,j}(\xi)d\xi\right)\exp\left(-\int_0^x \overline{\mu}_{lin,j}(\xi)d\xi\right). \tag{5}$$

The first term in the right side of Eq. (5) corrects for the absorption effects within the confocal volume. The second term corrects for the attenuation of the primary and secondary radiation on the path from the sample surface to the probing position x. This term does not depend on ζ and therefore it can be excluded from the main integral

$$\Phi_j(x) = \exp\left(-\int_0^x \overline{\mu}_{lin,j}(\xi)d\xi\right)\int_0^D G_j(\zeta, x)\rho_j(\zeta)d\zeta, \tag{6}$$

$$G_j(\zeta, x) = \eta_j'(\zeta - x)\exp\left(\int_\zeta^x \overline{\mu}_{lin,j}(\xi)d\xi\right). \tag{7}$$

Function $G_j(\zeta, x)$ takes into account the absorption effects within the probing volume. It can be considered as an expanded version of the original sensitivity function $\eta_j'(x)$. As shown in Eq. (7) the absorption of primary and secondary radiations inside the confocal volume modifies the original sensitivity function $\eta_j'(x)$ in a way that for $\zeta < x$ the sensitivity profile is enhanced by the exponent term which becomes > 1, whereas for $\zeta > x$ the exponent term becomes < 1 and the sensitivity profile is attenuated. The distortion of the original sensitivity function depends on the effective linear absorption coefficient as well as on the size of the confocal volume. In the case of weakly absorbing matrices and small probing volumes

$$\exp\left(\int_\zeta^x \overline{\mu}_{lin,j}(\xi)d\xi\right) \approx 1 \Rightarrow G_j(\zeta, x) \approx \eta_j'(\zeta - x). \tag{8}$$

In such a case Eq. (6) can be simplified to

$$\begin{aligned}\Phi_j(x) &= \exp\left(-\int_0^x \overline{\mu}_{lin,j}(\xi)d\xi\right)\int_0^D \eta_j'(\zeta - x)\rho_j(\zeta)d\zeta \\ &= \exp\left(-\int_0^x \overline{\mu}_{lin,j}(\xi)d\xi\right)(\eta_j' * \rho_j)(x).\end{aligned} \tag{9}$$

where operators $*$ and $\times$ are convolution and multiplication, respectively. The derived Eq. (9) opens up a possibility for determining the local density depth profile of the j-th element by a direct deconvolution of the observed X-ray fluorescence signal $\Phi_j(x)$ with known sensitivity function $\eta_j'(x)$ followed by the absorption correction of the deconvolved profile $\Phi_{j,deconvolved}(x)$

$$\Phi_j(x); \eta_j'(x) \overset{deconvolution}{\rightarrow} \Phi_{j,deconvolved}(x) = \exp\left(-\int_0^x \overline{\mu}_{lin,j}(\xi)d\xi\right)\rho_j(x), \tag{10}$$

$$\rho_j(x) = \Phi_{j,deconvolved}(x)\exp\left(\int_0^x \overline{\mu}_{lin,j}(\xi)d\xi\right) \tag{11}$$

$\Phi_{j,deconvolved}(x)$ is a dimension of density. The function $\eta_j'(x)$ must be known in advance, it can be determined by fitting Eq. (4) to the measured depth profile of a thin film standard sample. As shown in Eq. (11) the local density profile of the analyzed element is calculated by multiplying the deconvolved intensity profile by the exponential term determined at each probing position. This term is responsible for correcting the absorption effects due to the presence of absorbing layers of the sample between the current position of the probing volume and the sample surface. To convert the local density profiles $\rho_j(x)$ into profiles of the concentration we assume a known density of the matrix and known densities of the elements (or chemical compounds containing given element) mixed with the matrix. Assuming that the elements (compounds) are not diluted but mixed with the matrix one can calculate the overall sample density at given depth and use it to obtain concentration depth profiles.

The deconvolution with regularization procedure [17,18] was used to deconvolve the intensity profiles. In this procedure the analyzed signal h (the measured characteristic peak intensity profile) is a convolution of the known point spread function (PSF) g (the spectrometer sensitivity function) and the real signal f (the absorption modified element density profile) with superimposed noise n (statistical fluctuations of the measured intensity profile). The relation between these functions can be written in the following form:

$$h = f * g + n \tag{12}$$

where $*$ is a convolution operator. Function f is approximated by $\hat{f}$ which minimizes the following expression:

$$\sum_x \frac{((\hat{f} * g)(x) - h(x))^2}{n^2(x)} + \lambda\sum_x \left|\frac{\Delta\hat{f}(x)}{\Delta x}\right|. \tag{13}$$

The dimensionless λ parameter controls the strength of the regularization (smoothing). For given problem the value of this parameter has to be chosen empirically to get the best compromise between the smoothing and the maximization of goodness of fit. The first term in this sum governs how accurately the convolution of the approximated function $\hat{f}$ and the sensitivity function g fits to the signal h. The second term avoids solutions affected with high noise.

In the numerical implementation used in this work the measured and deconvolved signals were discrete functions of probing positions. The sample was divided into a stack of layers

with number of layers equal to the number of probing points. The thickness of each layer was equal to the step size of the confocal scan, Δx. The local densities of all detectable elements inside individual layers were calculated subsequently starting from the first layer (the surface layer of the sample facing the detector) for which there were no other absorbing layers on the paths toward the source and the detector. In the case of the first layer the absorption correction term in Eq. (11) was equal to 1 and the local density of the j-th element was calculated using

$$\rho_j(x_1) = \Phi_{j,deconvolved}(x_1). \quad (14)$$

For all subsequent layers the element density values were calculated taking into account absorption in all preceding layers

$$\rho_j(x_n) = \Phi_{j,deconvolved}(x_n)\exp\left(\Delta x \sum_{k=1}^{n-1}\sum_i \rho_i(x_k)\left(\frac{\mu_{0,i}}{\cos\phi} + \frac{\mu_{j,i}}{\cos\varphi}\right)\right). \quad (15)$$

To calculate the absorption correction for element j inside n-th layer the local densities of all elements in the preceding layers (detected elements and elements of dark matrix) have to be known. For this reason the composition and density of the sample matrix as well as chemical form of detected elements were assumed to be known. All calculations were performed with fundamental parameters taken from the *xraylib* library [19,20].

3. Experimental

The set of hypothetical single layer and multi-layered samples with assumed parameters/excitation conditions and two in-house produced multi-layered standards, measured at a synchrotron beam line, were used to validate the developed model. The multi-layered samples with low absorption of X-rays were chosen in order to allow the analysis within large range of depths.

The set of hypothetical single layer samples was based on homogenous layer containing zinc in polyethylene matrix with different effective linear absorption coefficients. The nominal composition and mass density of the samples are presented in Table 1. The synthetic intensity profiles of Zn-Kα line were generated for these samples by applying theoretical models given by Eqs (1) and (9) and utilizing two values of the σ_x parameter: 5 μm and 15 μm. The thickness of all samples was assumed to be equal to 150 μm. The energy of the exciting radiation was set to 20.5 keV, the values of the parameters $\tilde{\eta}$, and Φ_0 were set to 1.

A multi-layered hypothetical standard was defined to verify the reliability of the derived model given by Eq. (15). The sample was assumed to be composed of five layers containing different concentrations of copper and zinc in polyethylene matrix. The effective linear absorption coefficients varied from 4.3 cm^{-1} to 22.8 cm^{-1} for Zn-Kα line and from 5.2 cm^{-1} to 25.9 cm^{-1} for Cu-Kα line. The theoretical profiles of Cu-Kα and Zn-Kα peaks were calculated assuming 2.5 μm step size and utilizing the multi-layered sample formula derived in [12] based on the general model given by Eq. (1). The nominal composition of layers is presented in Table 2. The parameters $\tilde{\eta}$ and Φ_0 were set to 1, while $\sigma_{x,Cu-K\alpha}$ and $\sigma_{x,Zn-K\alpha}$ parameters were set to 6.5 μm and 6.0 μm, respectively.

The two in-house developed standards consisted of nine layers made of the Engage™ 8003 polyolefin elastomer doped with zinc or copper oxide powders with the nominal weight fractions of 4.5% for Cu_2O (4% of Cu) and 4.98% for ZnO (4% of Zn). The first sample consisted of five ZnO doped layers (odd numbered layers) separated with pure polymer matrix (even numbered layers), whereas the second one consisted of five ZnO doped layers (odd numbered layers) separated with Cu_2O doped layers (even numbered layers). The thicknesses of all layers were determined by the observation of cross sections of samples with an optical microscope. The effective linear absorption coefficient for Zn-Kα line varied from 4.3 cm^{-1} (pure matrix) to 8.7 cm^{-1} (ZnO doped layer) whereas for Cu-Kα line this quantity varied from 5.2 cm^{-1} (pure matrix) to 10.1 cm^{-1} (ZnO doped layer). The full description of these standards was given in [14]. The confocal experiment of these standards was performed at the beamline *L* [21] of the synchrotron storage ring DORIS III in the Hamburger Synchrotronstrahlungslabor (HASYLAB) at DESY, Hamburg, Germany. The monochromatic beam of exciting radiation with an energy of 20.5 keV was focused with a polycapillary half-lens to a spot size of 6.7 μm FWHM. A probing volume was formed by attaching polycapillary half-lens [22] to the detection channel in 45°/45° geometry. The spatial resolution of the probing volume (expressed as the σ_x of the registered depth-sensitive profile of infinitely thin standard sample) was 6.06 μm at the energy of Zn-Kα line and 6.42 μm at the energy of Cu-Kα. The fluorescence radiation was registered with a Vortex silicon drift detector with a crystal thickness of 350 μm, an active area of 50 mm^2 and the energy resolution of 140 eV at the Mn-Kα line. The flux of primary radiation impinging onto the focusing optics was monitored with an ionization chamber. The current of the ionization chamber was

Table 1
Quantitative comparison of full and simplified formula for X-ray fluorescence intensity for different absorbing samples.

Zinc concentration [%]	31.1	50.1	62.1	70.3	76.3	80.8
Mean mass density of sample [g/cm^3]	1.23	1.6	1.96	2.33	2.7	3.06
Effective linear absorption coefficient [cm^{-1}]	50	100	150	200	250	300
Chi-square for σ_x=5 μm	$1.3\cdot10^{-4}$	$3.3\cdot10^{-4}$	$6.5\cdot10^{-4}$	$1.1\cdot10^{-3}$	$1.8\cdot10^{-3}$	$2.7\cdot10^{-3}$
Chi-square for σ_x=15 μm	$8.5\cdot10^{-4}$	$4.4\cdot10^{-3}$	$1.3\cdot10^{-2}$	$3.0\cdot10^{-2}$	$5.9\cdot10^{-2}$	$1.1\cdot10^{-1}$

Table 2
The input and reconstructed structure of the hypothetical layered sample.

Layer #	Input values			Reconstructed values		
	Thickness [μm]	Cu concentration [%]	Zn concentration [%]	Thickness [μm]	Cu concentration [%]	Zn concentration [%]
1	100	–	5	100.2 ± 0.4	–	4.99 ± 0.05
2	50	10	–	50.0 ± 0.4	10.0 ± 0.2	–
3	25	–	–	24.8 ± 0.4	–	–
4	100	2.5	–	100.1 ± 0.4	2.51 ± 0.06	–
5	50	–	15	50.0 ± 0.9	–	14.8 ± 0.2

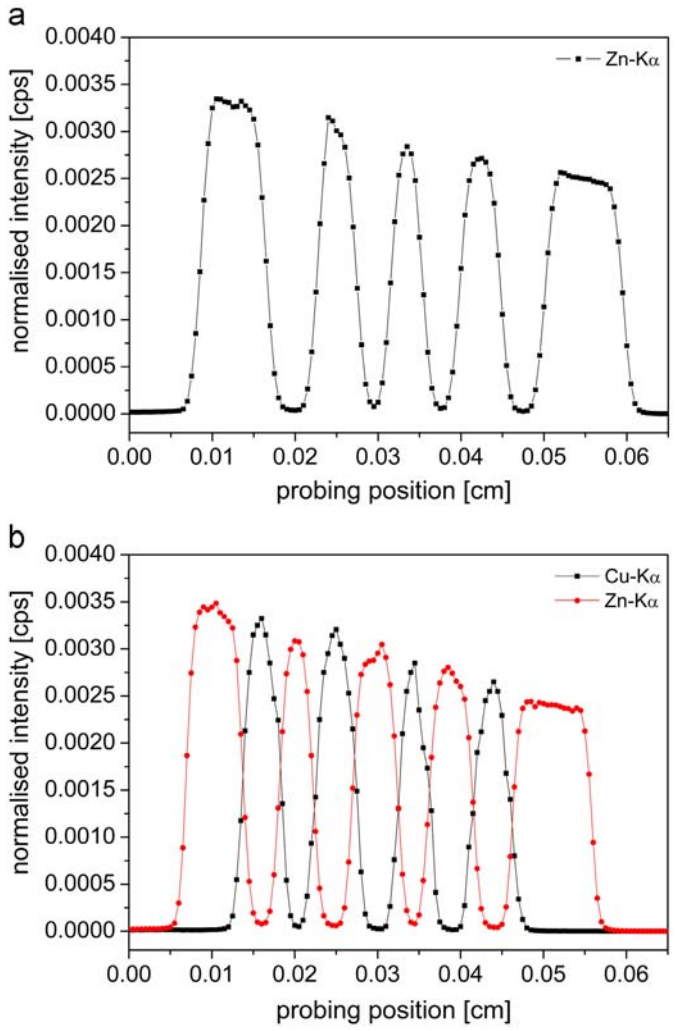

Fig. 1. (a) Averaged depth-sensitive intensity profiles of zinc for ZnO multi-layer sample. (b) Averaged depth-sensitive intensity profiles of zinc and copper for Cu_2O–ZnO multi-layer sample.

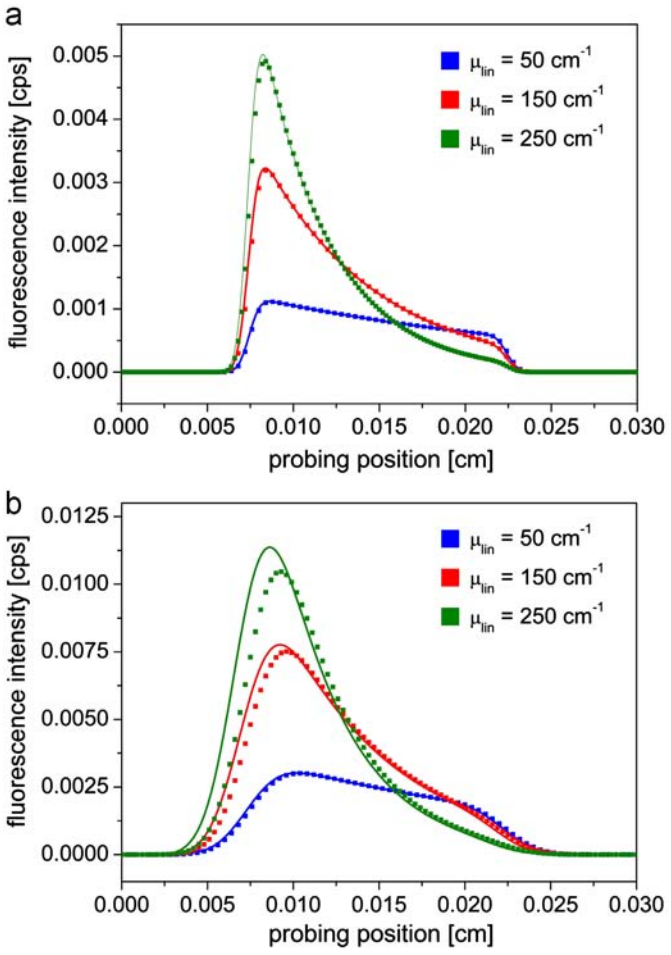

Fig. 2. (a) The comparison of general (dotted line) and simplified (solid line) formulas for the intensity of fluorescence radiation in confocal geometry for σ_x equal to 5 μm and different composition of the samples. The front of the sample is on the left side. (b) The comparison of general (dotted line) and simplified (solid line) formulas for the intensity of fluorescence radiation in confocal geometry for σ_x equal to 15 μm and different composition of the samples. The front of the sample is on the left side.

used for the normalization of experimental results. The standards were scanned in depth perpendicularly to the surface with a counting time of 5 s per point and with a step size of 5 μm in depth. A number of 36 lateral scans was executed in an area of 250 μm × 250 μm encompassing 4716 probing points for each sample. For each standard, the collected intensity depth profiles were averaged. The measured intensity profiles for both standards are presented in Fig. 1a,b. Analytical parameters of the confocal spectrometer were estimated by the measurements of thin multi-element NIST SRM 1832 and NIST SRM 1833 standards [23]. These reference materials were scanned in depth with a counting time of 10 s and a step size of 1 μm.

4. Results and discussion

The applicability range of the simplified model was examined by comparing the predicted profiles obtained with Eq. (9) to those generated with the general model given by Eq. (1) for the set of hypothetical single layer samples containing zinc in polyethylene matrix. The results of comparison are presented in Fig. 2a,b. The calculated reduced chi-square values for all compositions at both spatial resolutions are presented in Table 1. The results confirmed good agreement between the two models for samples with low

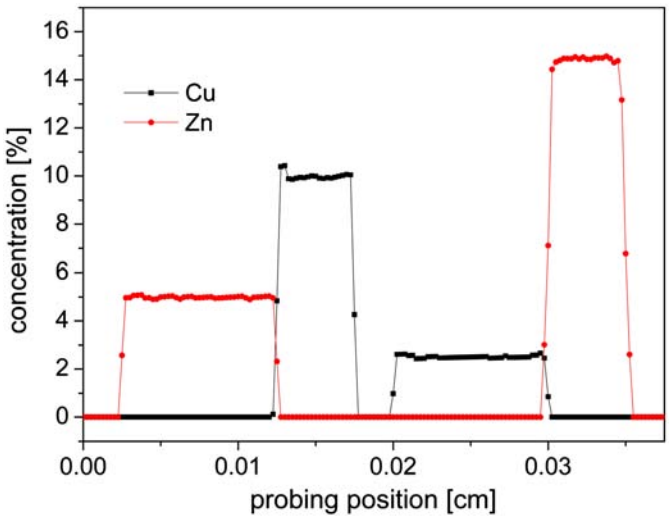

Fig. 3. Results of the quantification of synthetic sample. The front of the sample is on the left side.

effective linear coefficient (low density). Due to the fact that the exponential term in Eq. (7) was neglected in the simplified model given by Eq. (9) it was expected that significant discrepancy would

appear for large probing volumes and strong absorbing samples. The latter case may occur for samples with high mean atomic number and high mass density. The absorption is also stronger for low excitation energy and/or low fluorescent energy of analyzed element. For this reason the applicability of this simplified model may be limited for low energy X-ray fluorescence lines for which larger probing volumes are also introduced.,

For all multi-layer samples the positions of the layer borders with their uncertainties were estimated by fitting Gaussian functions to the first derivative of the concentration function of a given element. These values were then used to evaluate the thicknesses of layers and their uncertainties. The uncertainties of the chemical composition were estimated from the dispersion of the results within each layer.

The concentration profiles obtained for the multi-layered hypothetical standard, reconstructed by using the elaborated model given by Eq. (15), are shown in Fig. 3. The deconvolution procedure was carried out with the λ parameter equal to 0.0005. Reconstructed thicknesses and the mean composition of layers are shown in Table 2. As can be seen almost all estimates were in good agreement with input quantities. The concentration profiles of ZnO and Cu_2O in two in-house made multi-layered standards, were reconstructed by using the developed model and the average measured intensity profiles. The results are shown in Fig. 4a,b. The deconvolution was performed with λ parameter equal to 0.02. The results were compared with the results obtained with the Monte-Carlo simulation [13] and the general model given by Eq. (1) extended to multi-layered structures in [12]. The comparison of the nominal concentrations, thicknesses measured by an optical microscope and reconstructed quantities is presented in Tables 3 and 4. The reconstructed concentrations profiles of zinc and copper oxides obtained by the approach proposed in this work agreed very well with the estimates determined by existing quantification procedures and the nominal quantities. In almost all cases the determined estimates could be considered equal within the uncertainty interval. Relative uncertainties varied from 0.6% to 1.8% for ZnO doped layers and from 3.0% to 7.0% for Cu_2O doped layers. Greater uncertainties in the latter case resulted from less homogenous lateral distribution of copper oxide as compared to zinc. Due to the high counting statistics and the use of the averaged experimental depth-sensitive profiles, the contribution from the uncertainty of the measurement to the uncertainty of concentration was negligible. The deconvolution technique produced very small non-zero concentration estimates (equal to zero within uncertainty range) within the layers where the given element was not present The significant non-zero concentration appeared mainly for ZnO in Cu_2O doped layers—copper was not detected in ZnO doped layers. For this reason this effect could not be explained by any defect of the method—is such a case, it would be observable for both elements. Very likely explanation of this effect could be the diffusion of ZnO powder into Cu_2O doped layers that could be introduced during the sample preparation process.

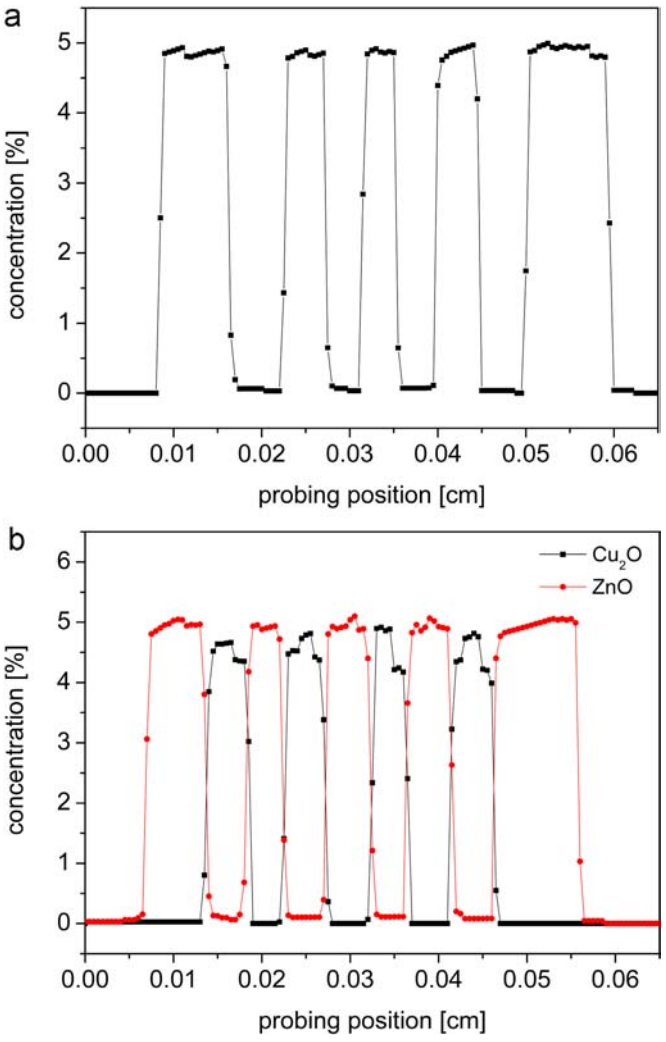

Fig. 4. (a) The reconstruction of the composition of ZnO multi-layer sample. The front of the sample is on the left side. (b) The reconstruction of the composition of Cu_2O–ZnO multi-layer sample. The front of the sample is on the left side.

5. Conclusions

A new quantification procedure for the determination of elemental concentration profiles in multi-layer samples examined by confocal X-ray fluorescence spectroscopy was derived and validated. The experimental verification proved very good performance of the proposed approach for weakly absorbing matrices.

Table 3
The reconstruction of thickness and composition of ZnO multi-layer sample obtained with three competitive quantification procedures.

Layer #	Thickness [μm]				Dopant concentration [%]			
	Optical microscopy	General model	MC simulation	Direct deconvolution	Nominal	General model	MC simulation	Direct deconvolution
1	80.3 ± 0.3	79.0 ± 0.7	80.5 ± 0.7	78.6 ± 0.6	4.98	4.2 ± 1.0	5.0 ± 0.1	5.0 ± 0.1
2	62.4 ± 0.5	62.2 ± 1.0	63.2 ± 0.5	62.4 ± 0.5	–	–	–	–
3	45.2 ± 0.4	45.5 ± 1.0	45.8 ± 0.4	46.5 ± 0.6	4.98	5.5 ± 1.3	5.1 ± 0.1	4.8 ± 0.1
4	43.5 ± 0.5	43.0 ± 1.1	43.8 ± 0.4	42.1 ± 0.7	–	–	–	–
5	38.8 ± 0.9	38.0 ± 1.1	38.7 ± 0.3	38.2 ± 0.7	4.98	5.7 ± 1.1	4.8 ± 0.2	5.0 ± 0.1
6	46.5 ± 0.6	45.0 ± 1.1	45.8 ± 0.4	43.8 ± 0.6	–	–	–	–
7	51.3 ± 1.1	49.0 ± 1.2	49.9 ± 0.4	49.6 ± 0.4	4.98	6.2 ± 1.4	4.8 ± 0.1	4.9 ± 0.1
8	54.8 ± 0.5	53.6 ± 1.2	55.0 ± 0.5	54.3 ± 0.4	–	–	–	–
9	97.3 ± 0.6	94.7 ± 1.2	96.8 ± 0.8	93.8 ± 0.7	4.98	7.2 ± 1.2	4.9 ± 0.1	4.9 ± 0.1

Table 4
The reconstruction of thickness and composition of Cu_2O–ZnO multi-layer sample obtained with three competitive quantification procedures.

Layer #	Thickness [μm]				Dopant concentration [%]			
	Optical microscopy	General model	MC simulation	Direct deconvolution	Nominal	General model	MC simulation	Direct deconvolution
1	67.5 ± 0.6	66.9 ± 0.6	69.3 ± 0.6	67.6 ± 0.6	4.98	5.1 ± 0.2	5.0 ± 0.1	4.9 ± 0.1
2	43.75 ± 0.5	45.1 ± 0.8	46.5 ± 0.4	48.8 ± 0.7	4.5	4.3 ± 0.5	4.7 ± 0.2	4.5 ± 0.3
3	42.3 ± 0.4	41.6 ± 0.8	43.4 ± 0.4	40.7 ± 0.4	4.98	4.5 ± 0.8	4.7 ± 0.2	4.9 ± 0.1
4	49.6 ± 0.6	48.3 ± 0.8	49.6 ± 0.5	45.6 ± 1.0	4.5	4.8 ± 0.8	4.8 ± 0.2	4.6 ± 0.2
5	51.9 ± 1.0	52.2 ± 0.8	53.8 ± 0.5	50.6 ± 0.4	4.98	6.2 ± 1.0	5.2 ± 0.2	4.9 ± 0.1
6	39.4 ± 0.9	38.0 ± 0.8	39.3 ± 0.4	40.3 ± 1.3	4.5	5.4 ± 0.8	4.6 ± 0.1	4.7 ± 0.4
7	52.1 ± 1.0	52.6 ± 0.8	54.8 ± 0.5	51.7 ± 0.7	4.98	6.4 ± 1.9	5.2 ± 0.1	4.9 ± 0.1
8	48.2 ± 0.6	47.3 ± 0.8	48.6 ± 0.5	49.2 ± 1.0	4.5	6.2 ± 1.1	4.8 ± 0.2	4.5 ± 0.3
9	98.0 ± 0.4	96.6 ± 0.9	100.3 ± 0.9	95.4 ± 0.5	4.98	7.6 ± 1.0	5.1 ± 0.2	5.0 ± 0.1

As compared to other methods of quantitative analysis the advantage of the proposed method is its simplicity. Moreover the direct deconvolution approach does not assume any structure of the sample and initial values are unnecessary. Furthermore, the direct deconvolution of position dependent X-ray fluorescence signal can be extended into the case of generally heterogeneous structures where the absorption correction is performed on a voxel by voxel way [24].

Acknowledgments

The authors would like to cordially acknowledge the advice and help received from Dr. Dariusz Wegrzynek, a staff member of the Faculty of Physics and Applied Computer Science, AGH University of Science and Technology, Krakow, Poland in verifying the underlying theoretical assumptions of the proposed model, and his willingness in reviewing our work.

The research was financially supported and realized under the auspices of the International Atomic Energy Agency, Vienna, Austria within the frame of research Contract no. 16023.

Portions of this research were carried out at the light source DORIS III at DESY, Hamburg, Germany, a member of the Helmholtz Association. Authors kindly thank Dr. Karen Appel for her assistance during the measurement session.

The computational part of the research was performed in the ACC CYFRONET AGH, Krakow, Poland within computational Grant no. MNiSW/IBM_BC_HS21/AGH/095/2009.

The research has received funding from the European Community's Seventh Framework Programme (FP7/2007-2013) under grant agreement no. 226716. The research was also supported by the Polish Ministry of Science and Higher Education and its grants for scientific research.

References

[1] W.M. Gibson, M.A. Kumakhov, SPIE Proc. 1736 (1993) 172.
[2] R.D. Perez, H.J. Sanchez, C.A. Perez, M. Rubio, Radiat. Phys. Chem. 79 (2010) 195–200.
[3] B. Kanngieer, W. Malzer, I. Reiche, Nucl. Instrum. Methods Phys. Res. B 211 (2003) 259–264.
[4] K. Nakano, K. Tsuji, X-Ray Spectrom. 38 (2009) 446–450.
[5] V. Mazel, I. Reiche, V. Busignies, P. Walter, P. Tchoreloff, Talanta 85 (2011) 556–561.
[6] P. Wrobel, M. Czyzycki, L. Furman, K. Kolasinski, M. Lankosz, A. Mrenca, L. Samek, D. Wegrzynek, Talanta 93 (2012) 186–192.
[7] I. Mantouvalou, K. Lange, T. Wolff, D. Grötzsch, L. Lühl, M. Haschke, O. Hahn, B. Kanngieer, J. Anal. At. Spectrom. 25 (2010) 554–561.
[8] K. Tsuji, K. Nakano, X. Ding, Spectrochim. Acta Part B 62 (2007) 549–553.
[9] L. Vincze, B. Vekemans, F.E. Brenker, G. Falkenberg, K. Rikers, A. Samogyi, M. Kersten, F. Adams, Anal. Chem. 76 (2004) 6786.
[10] Z. Smit, K. Janssens, K. Proost, I. Langus, Nucl. Instrum. Methods Phys. Res. B 219 (2004) 35.
[11] W. Malzer, B. Kanngieβer, Spectrochim. Acta Part B 60 (2005) 1334–1341.
[12] I. Mantouvalou, W. Malzer, I. Schaumann, L. Luhl, R. Dargel, C. Vogt, B. Kanngiesser, Anal. Chem. 80 (2008) 819–826.
[13] M. Czyzycki, D. Wegrzynek, P. Wrobel, M. Lankosz, X-Ray Spectrom. 40 (2011) 88–95.
[14] M. Czyzycki, P. Wrobel, M. Szczerbowska-Boruchowska, B. Ostachowicz, D. Wegrzynek, M. Lankosz, X-Ray Spectrom. 41 (2012) 273–278.
[15] W. Malzer, B. Kanngieer, X-Ray Spectrom. 32 (2003) 106–112.
[16] T. Schoonjans, G. Silversmit, B. Vekemans, S. Schmitz, M. Burghammer, C. Riekel, F.E. Brenker, L. Vincze, Spectrochim. Acta Part B 67 (2012) 32–42.
[17] W. Stefan, E. Garnero, R.A. Renaut, Geophys. J. Int. 167 (2006) 1353–1362.
[18] C.R. Vogel, Comput. Methods Inverse Probl., SIAM, Front. Appl. Math. (2002).
[19] A. Brunetti, M. Sanchez del Rio, B. Golosio, A. Simionovici, A. Somogyi, Spectrochim. Acta 59B (2004) 1725.
[20] T. Schoonjans, A. Brunetti, B. Golosio, M. Sanchez del Rio, V.A. Sole, C. Ferrero, L. Vincze, Spectrochim. Acta 66B (2011) 776.
[21] G. Falkenberg, O. Clauss, A. Swiderski, T. Tschentscher, X-Ray Spectrom. 30 (2001) 170.
[22] G. Falkenberg, Hasylab Annu. Rep. (2007).
[23] P.A. Pella, D.E. Newbury, E.B. Steel, D.H. Blackburn, Anal. Chem. 58 (1986) 1133.
[24] I. Szaloki, A. Gerenyi, T. Schoonjans, B. De Samber, L. Vincze, in: Christina Streli, Andrzej Markowicz (Eds.), Proceedings of EXRS 2012 European Conference on X-ray Spectrometry Program and Book of Abstracts, Vienna, Austria, June 18–22, 2012, p. 88.